Title	Constitutive aryl hydrocarbon receptor signaling constrains type I interferon-mediated antiviral innate defense
Author(s)	Yamada, Taisho; Horimoto, Hiromasa; Kameyama, Takeshi; Hayakawa, Sumio; Yamato, Hiroaki; Dazai, Masayoshi; Takada, Ayato; Kida, Hiroshi; Bott, Debbie; Zhou, Angela C; Hutin, David; Watts, Tania H; Asaka, Masahiro; Matthews, Jason; Takaoka, Akinori
Citation	Nature Immunology, 17(6), 687-694 https://doi.org/10.1038/ni.3422
Issue Date	2016-06
Doc URL	http://hdl.handle.net/2115/63086
Type	article (author version)
Note	Supplementary materials are available on the publisher's website.
File Information	NatImmunol17_687.pdf ()

Instructions for use

Constitutive aryl hydrocarbon receptor signaling constrains type-I-interferon-mediated antiviral innate defense

Taisho Yamada[1,11], Hiromasa Horimoto[1,2,11], Takeshi Kameyama[1,3], Sumio Hayakawa[1,3], Hiroaki Yamato[1,2], Masayoshi Dazai[1,2], Ayato Takada[4,5], Hiroshi Kida[5,6], Debbie Bott[7], Angela C Zhou[8], David Hutin[7], Tania H Watts[8], Masahiro Asaka[9], Jason Matthews[7,10] & Akinori Takaoka[1,3]

[1]*Division of Signaling in Cancer and Immunology, Institute for Genetic Medicine, Hokkaido University, Sapporo, Japan.* [2]*Department of Gastroenterology, Hokkaido University Graduate School of Medicine, Sapporo, Japan.* [3]*Molecular Medical Biochemistry Unit, Graduate School of Chemical Sciences and Engineering, Hokkaido University, Sapporo, Japan.* [4]*Division of Global Epidemiology, Research Center for Zoonosis Control, Hokkaido University, Sapporo, Japan.* [5]*Global Station for Zoonosis Control, Global Institution for Collaborative Research and Education, Hokkaido University, Sapporo, Japan .* [6]*Laboratory of Microbiology, Department of Disease Control, Graduate School of Veterinary Medicine, Hokkaido University, Sapporo, Japan.* [7]*Department of Pharmacology and Toxicology, University of Toronto, Toronto, Ontario, Canada.* [8]*Department of Immunology, University of Toronto, Toronto, Ontario, Canada.* [9]*Health Sciences University of Hokkaido,Toubetu, Japan.* [10]*Department of Nutrition, Institute of Basic Medical Sciences, University of Oslo, Oslo, Norway.* [11]*These authors contributed equally to this work. Correspondence should be addressed to A. Takaoka. (takaoka@igm.hokudai.ac.jp)*

Aryl hydrocarbon receptor (AHR) is a ligand-activated transcription factor that mediates the toxic activity of many environmental xenobiotics. However, its role in innate immune responses during viral infection is not fully understood. Here we demonstrate that constitutive AHR signaling negatively regulates the type I interferon (IFN-I) response during infection with various types of virus. Virus-induced IFN-β production was enhanced in AHR-deficient cells and mice and resulted in restricted viral replication. We found that AHR upregulates expression of the ADP-ribosylase TIPARP, which in turn causes downregulation of the IFN-I response. Mechanistically, TIPARP interacted with the kinase TBK1 and suppressed its activity by ADP-ribosylation. Thus, this study reveals the physiological importance of endogenous activation of AHR signaling in shaping the

1

IFN-I-mediated innate response and, further, suggests that the AHR-TIPARP axis is a potential therapeutic target for enhancing antiviral responses.

AHR was originally discovered as a xenobiotic sensor that mediates the toxicity of the persistent environmental contaminant, 2,3,7,8-tetrachlorodibenzo-*p*-dioxin (TCDD), more commonly known as dioxin[1–4]. Activation of AHR induces its target genes, including those encoding cytochrome P4501A1, cytochrome P4501B1, AHR repressor, TCDD-inducible poly(ADP-ribose)polymerase (TIPARP) and aldehyde dehydrogenase 1A3 (refs. 1,2,5–9), which are involved in the adaptive metabolism of xenobiotic compounds. This property of AHR has been implicated in host defense against bacterial infection, as certain bacterial pigmented virulence factors are AHR agonists that are subsequently metabolized by AHR-regulated drug-metabolizing enzymes[10]. Studies of AHR-deficient mice have identified important physiological roles for AHR in response to endogenous ligands in cell cycle regulation, cell differentiation and immune responses[8,11–14]. In relation to this, several putative endogenous ligands for the AHR have also been reported, including heme metabolites, arachidonic acids or leukotrienes and tryptophan metabolites, such as 6-formylindolo(3,2-*b*)carbazole (FICZ) and kynurenine (Kyn)[2,8,15].

There has been increased interest in understanding the role of AHR in immunity. Several reports, most of which are based mainly on experiments with dioxin treatment, have shown that the AHR is involved in the differentiation and/or function of T cells, macrophages and dendritic cells[7,9,11,16–21]. AHR has been implicated in the control of acute graft-versus-host disease and autoimmunity[11,12,21]. Dioxin-activated AHR also reduces the survival rate of mice infected with influenza A virus[22,23] and indirectly suppresses the proliferation and differentiation of virus-specific $CD8^+$ T cells via its regulatory role in dendritic cells[24]. FICZ and dioxin diminish $CD8^+$ T cell responsiveness, whereas dioxin, but not FICZ, affects neutrophil recruitment or pulmonary inducible nitric oxide synthase (iNOS) induction in response to influenza virus infection[25].

Tryptophan metabolites such as Kyn are upregulated during inflammation and/or tumor progression in several types of immune and tumor cells through the catalytic activity of tryptophan dioxygenase (TDO) and indoleamine 2,3-dioxygenase (IDO), which catalyze the first step in the formation of Kyn from tryptophan[2,9]. This increase in Kyn leads to an increase in regulatory T cells (T_{reg} cells), inducing immune tolerance[26].

However, there are limited of studies investigating the role of constitutive AHR signaling by endogenous ligands for the regulation of immune responses.

We focused here on the effect of constitutive AHR signaling on IFN-I, a crucial player in the innate immune response that confers an antiviral state in cells on viral infection[27]. IFN-I is strongly induced after the activation of a subset of pattern-recognition receptors (PRRs), such as RIG-I, through their recognition of virus-derived nucleic acids[28–31]. RIG-I and cyclic GMP-AMP synthase (cGAS) are cytosolic RNA and DNA sensors, respectively, that induce IFN-I production through a common pathway involving the kinase TBK1 and the transcription factor IRF-3 (refs. 27–36).

In the present study we found that the IFN-I response was markedly enhanced in AHR-deficient cells during infection with various types of virus. We also identified TIPARP as an AHR target that post-translationally ADP-ribosylates TBK1, playing an essential part in AHR-mediated regulation of IFN-I production. Our findings thus demonstrate a link between AHR signaling and innate signaling for the modulation of interferon-mediated antiviral response during viral infection.

RESULTS

Endogenous AHR signaling modulates IFN-I response

We first examined the involvement of AHR in a virally induced IFN-I response. Compared to wild-type mouse embryonic fibroblasts (MEFs), AHR-deficient ($Ahr^{-/-}$) MEFs showed marked enhancement of the IFN-I response against infection with RNA and DNA viruses including vesicular stomatitis virus (VSV), influenza virus (A/Puerto Rico/8/1934 H1N1 strain) (FluV), Newcastle disease virus (NDV), Sendai virus (SeV), encephalomyocarditis virus (EMCV) and herpes simplex virus-1 (HSV-1) (**Fig. 1a** and **Supplementary Fig. 1a**). Similar observations were made in $Ahr^{-/-}$ MEFs stimulated with microbial-associated molecular patterns (MAMPs; 5'-triphosphate RNA (3pRNA), poly(rI:rC) and double-stranded vaccinia virus (dsVACV) 70-mer) (**Supplementary Fig. 1b,c**). This phenotype was rescued by overexpression of wild-type AHR in $Ahr^{-/-}$ MEFs (**Supplementary Fig. 1c,d**). We also found that AHR deficiency enhanced the phosphorylation of TBK1 and IRF-3, essential mediators of IFN-I production

(**Supplementary Fig. 1e**). Consistent with the enhanced IFN-I response, viral titers were significantly reduced in $Ahr^{-/-}$ MEFs at 24 h after infection with VSV or FluV (**Fig. 1b**). We next evaluated the functional role of AHR in bone-marrow-derived macrophages (BMDMs) and splenocytes derived from wild-type and $Ahr^{-/-}$ mice. Similarly to our findings with MEFs, IFN-β production was higher in $Ahr^{-/-}$ BMDMs than in wild-type cells after FluV infection or nucleic acid stimulation (3pRNA or extracellular poly(rI:rC)) (**Fig. 1c** and **Supplementary Fig. 1f**,**g**).

In addition, $Ahr^{-/-}$ C57BL/6N mice showed increased IFN-β protein at 36 h after FluV infection, and this was accompanied by markedly reduced viral titers (**Fig. 1d**). The expression of several AHR target genes was significantly lower ($P < 0.01$, Student's t-test) in $Ahr^{-/-}$ MEFs than in wild-type MEFs, and consistently, their expression levels were also reduced in wild-type MEFs treated with the AHR-specific antagonist CH-223191 (ref. 37) compared with the control group (DMSO) (**Supplementary Fig. 1h**), suggesting that AHR signaling is constitutively activated. We next examined whether the AHR-mediated effect on IFN-I response was dependent on its endogenous ligand(s). CH-223191 treatment upregulated the IFN-β response to viral infection or stimulation with 3pRNA or cyclic GMP-AMP (cGAMP) (**Fig. 1e** and **Supplementary Fig. 1i**,**j**). These results suggest that IFN-I production in response to viral infection is negatively regulated by endogenously activated AHR signaling. In support of this idea, the IFN-I response to infection with viruses or stimulation with 3pRNA was significantly suppressed by treatment with endogenous AHR ligands Kyn or FICZ (**Fig. 2a**,**b** and **Supplementary Fig. 2a**). In contrast, IFN-β production in response to VSV infection was upregulated in wild-type MEFs after pretreatment with 680C91, a specific inhibitor of TDO that catalyzes the first step in the formation of Kyn from tryptophan[38] (**Fig. 2c** and **Supplementary Fig. 2b**), an effect not observed in $Ahr^{-/-}$ MEFs (**Fig. 2c**). We obtained similar results in $Ahr^{-/-}$ BMDMs on treatment with an IDO inhibitor (1-MT) (**Supplementary Fig. 2c**). Moreover, intraperitoneal (i.p.) pretreatment with FICZ resulted in a marked reduction in serum IFN-β protein at 12 h after VSV infection in wild-type mice, which was consistent with elevated viral titers (**Fig. 2d**), whereas this effect was not observed in $Ahr^{-/-}$ mice (**Fig. 2d**). VSV infection did not seem to activate AHR signaling during the early phase of infection, which is consistent with the observation that AHR-inducible genes such as *Cyp1a1* (encoding cytochrome P4501A1)

were not upregulated in response to VSV infection, whereas interferon-inducible genes, including *Oas1a* and *Rsad2*, were induced (**Supplementary Fig. 2d**). Taken together, these results indicate that constitutive activation of AHR signaling by endogenous ligands modulates IFN-I production pathway *in vitro* and *in vivo* during viral infection.

AHR negatively regulates antiviral response via TIPARP

To clarify whether this suppressive effect is mediated directly or indirectly through ligand-dependent activation of AHR, we used cycloheximide (CHX) as a protein synthesis inhibitor. We found that Kyn did not suppress 3pRNA-induced *Ifnb1* mRNA induction (**Supplementary Fig. 2e**), suggesting that Kyn negatively regulates the interferon response possibly via induction of one or more AHR target genes. We next examined the possible involvement of several representative AHR-inducible genes in the suppression of 3pRNA-induced interferon response by knockdown using small interfering RNAs (siRNAs) in MEFs (**Supplementary Fig. 2f**). Knockdown of TIPARP (siTIPARP) abolished the suppressive effect of Kyn on *Ifnb1* induction in MEFs (**Fig. 3a**). These results suggest that TIPARP may be a key mediator in AHR signaling to negatively modulate virally induced interferon response.

We focused on TIPARP because it catalyzes ADP-ribosylation of proteins and is classified in the CCCH-poly(ADP-ribose) polymerase (CCCH-PARP) subfamily[6,39–42], another member of which, ZC3HAV1, engages in host defense against viral infection[41,42]. We observed upregulation of *Tiparp* mRNA in mouse and *TIPARP* mRNA in human cells after treatment with endogenous AHR ligands Kyn or FICZ (**Fig. 3b** and **Supplementary Fig. 2g**). The expression of mRNA encoding other representative PARP family members (*Parp1*, *Parp2*, *Parp9*, *Parp12* and *Zc3hav1*) was not increased after treatment with Kyn or FICZ (**Supplementary Fig. 2h**). In addition, we observed upregulation of TIPARP *in vivo* in FICZ-treated wild-type C57BL/6N mice (**Supplementary Fig. 2i**). We also found that the expression of *Tiparp* mRNA was abolished in *Ahr*^{−/−} MEFs, suggesting that the induction of TIPARP is dependent on AHR (**Fig. 3c**). To examine the functional role of TIPARP in the IFN-I production pathway, we exogenously expressed TIPARP in HEK293T cells, which resulted in suppression of interferon response to NDV infection (**Fig. 3d**) or 3pRNA stimulation (**Supplementary Fig. 3a,b**). No such effect was observed for IL-1β□nduced *IL8* expression in HEK293T

cells (**Supplementary Fig. 3c**). *IFNB1* mRNA was strongly upregulated by knockdown of *TIPARP* expression in HEK293T cells treated with 3pRNA (**Supplementary Fig. 3d**). This siRNA-mediated effect was rescued by expression of mouse TIPARP (**Fig. 3e**), which was not targeted by this siRNA but was functional in human cells (data not shown).

We further analyzed TIPARP-deficient (*Tiparp*$^{-/-}$) MEFs to investigate the role of TIPARP in negatively regulating the IFN-I response. *Ifnb1* mRNA and IFN-β protein were considerably upregulated in *Tiparp*$^{-/-}$ MEFs (compared with wild-type MEFs) after stimulation with all of the nucleic acid ligands tested (**Fig. 4a**,**b** and **Supplementary Fig. 3e**). Consistent with these results, the IFN-β response was enhanced in *Tiparp*$^{-/-}$ MEFs after infection with NDV, FluV and VSV (which activate RIG-I); EMCV (which activates melanoma differentiation-associated protein Mda5) and HSV-1 (which activates cGAS)[36,43] (**Fig. 4c**,**d**). The IFN-β response in *Tiparp*$^{-/-}$ BMDMs was also enhanced, as compared with wild-type cells, upon FluV infection or poly(rI:rC) stimulation (**Fig. 4e** and **Supplementary Fig. 3f**). These findings are in line with the observation that viral titers at 24 h after infection with any of these viruses were much lower in *Tiparp*$^{-/-}$ MEFs than in wild-type MEFs (**Fig. 4f**). Taken together, our data indicate that TIPARP functions as a critical regulator to suppress the interferon antiviral response activated by nucleic acid sensors after infection with a wide range of viruses.

TIPARP suppresses TBK1 activity via ADP-ribosylation

Next, we examined which step of the RIG-I signaling pathway TIPARP acts on. Activation of the *IFNB1* promoter by overexpression of N-terminal RIG-I and its adaptor MAVS or the downstream TBK1 was markedly suppressed in TIPARP-expressing HEK293T cells, whereas such suppression was not observed with overexpression of a constitutively active IRF-3 mutant (IRF-3/5D)[44] (**Fig. 5a**). Moreover, the TBK1-induced dimer formation of IRF-3, a key transcription factor for interferon induction[27], was enhanced in *Tiparp*$^{-/-}$ MEFs compared with wild-type MEFs (**Fig. 5b**). This suggests that TIPARP acts on TBK1 to suppress IFN-I induction. Therefore, we focused on the involvement of TIPARP in TBK1 activation to further determine the molecular mechanism underlying the TIPARP-involved regulation of nucleic acid–triggered signaling. Because TIPARP is an enzyme that post-translationally modifies itself and

other proteins, including AHR[39,40], we further investigated the relationship between TIPARP and TBK1, including their physical interaction. Endogenous TBK1, but not IRF-3, interacted with endogenous TIPARP after 3pRNA stimulation (**Fig. 5c**). In addition, recombinant TIPARP protein was pulled down with recombinant TBK1 protein, which indicates a direct interaction between these proteins (**Supplementary Fig. 4a**). Consistent with these findings, confocal microscopy revealed that YFP-tagged TIPARP colocalized with endogenous TBK1 in the perinuclear region in a ligand-dependent manner (**Fig. 5d** and **Supplementary Fig. 4b**). We next performed nuclear and cytosolic protein fractionation to examine the distribution of TIPARP after 3pRNA stimulation. 3pRNA stimulation resulted in increased TIPARP protein in the cytosolic fraction, which was reduced by treatment with leptomycin B, an inhibitor of nuclear export (**Supplementary Fig. 4c**). This suggests that 3pRNA stimulation at least partly facilitates the nuclear export of TIPARP, which is then able to interact with and regulate TBK1 activity. An N-terminal TBK1 mutant encompassing only its kinase domain (TBK1(KD)) showed much stronger binding activity to HA-tagged TIPARP than did the full-length TBK1 (TBK1(WT)) or a C-terminal mutant (TBK1(ULD+CC)) (**Supplementary Fig. 4d**), which suggests that this interaction is predominantly mediated through the TBK1 kinase domain. On the other hand, the coimmunoprecipitation with several TIPARP deletion mutants showed that the C-terminal TIPARP region containing all of the known domains (C-TIPARP) but not its N-terminal 236-aa region (N-TIPARP) is required for the interaction with TBK1 (**Supplementary Fig. 4e**). We next determined whether TIPARP regulates the autophosphorylation of TBK1 at S172, which is crucial for its activation[45]. Time-course analysis showed that both S172 of TBK1 and S396 of IRF-3 were phosphorylated to a greater degree in *Tiparp*^{−/−} MEFs than in wild-type MEFs after VSV infection or 3pRNA stimulation (**Fig. 5e** and **Supplementary Fig. 4f**). As reported[40], TIPARP showed auto-mono-ADP-ribosyltransferase activity. Recombinant TBK1 protein underwent ADP-ribosylation in the presence of recombinant intact TIPARP (rGST-TIPARP(WT)) but not the catalytically inactive mutant rGST-TIPARP(H532A) (**Fig. 5f**), suggesting that the ADP-ribosylation of TBK1 is dependent on the catalytic activity of TIPARP. In addition, TBK1 was ADP-ribosylated in virally infected or 3pRNA-stimulated wild-type MEFs, whereas ADP-ribosylation was not detected in *Tiparp*^{−/−} MEFs (**Fig. 5g** and **Supplementary Fig. 5a,b**). We also determined that the TBK1(KD) was ADP-ribosylated by TIPARP (**Supplementary Fig.**

5c), suggesting that the ADP-ribosylation of TBK1(KD) might hinder the autophosphorylation of TBK1. Consistent with these results, incubation of TBK1 with rGST-TIPARP(WT) but not rGST-TIPARP(H532A) resulted in suppression of autophosphorylation (at S172) of TBK1 (**Fig. 5h**). This result prompted us to further investigate whether the suppressive effect of TIPARP on the interferon response is based on its enzymatic activity. Whereas the reconstitution of wild-type TIPARP in *Tiparp*$^{-/-}$ MEFs could rescue the knockout phenotype for IFN-I response to FluV infection or ligand stimulation (3pRNA, poly(rI:rC) or dsVACV 70-mer), the enzymatic inactive mutant TIPARP(H532A) did not (**Fig. 5i** and **Supplementary Fig. 5d**,**e**). Consistent with this, virus titers were also restored by the introduction of intact TIPARP but not the TIPARP(H532A) in *Tiparp*$^{-/-}$ MEFs (**Fig. 5i**). These data suggest that TIPARP modifies TBK1 activity via ADP-ribosylation of the TBK1 protein, resulting in the suppression of IRF-3-mediated IFN-I induction.

AHR-TIPARP axis contributes to IFN-I antiviral response

Last, we determined whether AHR signaling is crucially involved in the regulation of virally induced interferon response through the induction of TIPARP. In contrast to the data above (**Fig. 2a,b**), Kyn and FICZ did not suppress *Ifnb1* mRNA induction by 3pRNA stimulation or FluV infection in *Tiparp*$^{-/-}$ MEFs (**Fig. 6a**). Additionally, we examined the role of TIPARP, which is induced by constitutive activation of AHR signaling by endogenous ligands (**Supplementary Fig. 1h**). We observed that virally induced IFN-β production was not affected by blockade of AHR signaling with CH-223191 in *Ahr*$^{-/-}$ MEFs or *Tiparp*$^{-/-}$ MEFs (**Fig. 6b**). A similar result was obtained when the Kyn was reduced by treatment with the TDO inhibitor 680C91 (**Supplementary Figs. 2b** and **5f**). Consistent with these results, FluV titers were not suppressed in *Ahr*$^{-/-}$ or *Tiparp*$^{-/-}$ MEFs treated with CH-223191 (**Fig. 6c**). Furthermore, i.p. administration of CH-223191 caused a significant decrease ($P < 0.01$) of *Tiparp* mRNA in mouse lung tissue (**Supplementary Fig. 5g**) and led to enhanced IFN-β production during FluV infection, which was accompanied with significantly lower viral titers and better survival rates compared with controls injected with corn oil (**Fig. 6d**,**e**). We further evaluated *Tiparp*$^{-/-}$ mice to show the *in vivo* role of TIPARP in the negative regulation mediated by constitutive AHR signaling. Pharmacological inhibition of AHR signaling by CH-223191 treatment in *Tiparp*$^{-/-}$ mice did not affect IFN-β production (**Fig.**

6f). These results indicate that optimal induction of interferon-mediated antiviral response is dependent on TIPARP expression through constitutive AHR signaling mediated by endogenous ligand(s) (**Supplementary Fig. 6**).

DISCUSSION

This study demonstrates a physiological role of AHR-mediated signaling in the host antiviral defense system. Our analyses with AHR-deficient cells reveal that the AHR is a key regulator of IFN-I production activated by nucleic acid sensor–mediated signaling during infection with a variety of viruses, suggesting a novel relationship between AHR signaling and innate signaling. In addition, our results indicate that the constitutive AHR signaling mediated by endogenous ligands such as Kyn has a regulatory role in the virally induced interferon response. We also identified TIPARP, an ADP-ribosyltransferase, as a critical target induced by constitutively active AHR signaling. We showed that TIPARP is a suppressive regulator of the TBK1-mediated pathway, a cardinal pathway for interferon induction, possibly via its post-translational modification of the kinase domain of TBK1 by ADP-ribosylation. The kinase domain of TBK1 was shown to be targeted by TIPARP, leading to the suppression of TBK1 activity. The detailed mapping of the ADP-ribosylated sites of TBK1 is an important issue to be addressed to clarify this mechanism. Although TBK1 activity is regulated in a variety of ways, such as phosphorylation and ubiquitination[46], the ADP-ribosylation of TBK1 described here represents the first report, to our knowledge, of a mechanism for its regulation. In this regard, TIPARP catalytic activity could also be considered another therapeutic focus to modulate TBK1 kinase activity for the control of inflammation and cancer.

This study provides a physiological importance for AHR-regulated TIPARP expression in tuning the interferon response against viral infection, indicating a novel aspect of constitutive AHR signaling in innate immunity. Mechanisms must be in place to prevent deleterious host reactions to microbial infection, such as superfluous activation of inflammation or cytokine storms[31]. Our findings suggest that constitutive AHR signaling may help to protect the host from harmful effects caused by excessive IFN-I activation by modulating TIPARP expression to downregulate activation of TBK1 induced by the innate sensing of viral MAMPs, which are abundantly generated during infection with most viruses. Alternatively, our results suggest the possibility that AHR activation by

intrinsic factors produced after stress or by nutritional dysregulation is responsible for the attenuation of innate resistance against viral infection. Our findings may thus have clinical applications, particularly for controlling pathological innate immune responses. In addition, our analyses with an AHR antagonist, a TDO inhibitor and an IDO inhibitor suggest that this constitutive AHR signaling is dependent on endogenous ligands including, possibly, tryptophan metabolites. It will be important to identify these endogenous AHR ligands and any factors that regulate tryptophan metabolism.

Given the constraining effect of AHR-induced TIPARP in virally induced interferon responses, it would be presumed that the AHR-TIPARP axis is hijacked on exposure to xenobiotic AHR ligands such as TCDD or 3-MC, which provides some insight into the understanding of their immunotoxicity[22,23]. The role of AHR during viral infection has so far been investigated mainly on the basis of analyses with exogenous ligands such as TCDD. Mouse survival rates after influenza virus infection are reduced by TCDD-induced AHR activation[22,23]. TCDD increases the replication of human cytomegalovirus, possibly through the dependence on AHR[47]. 3-MC induces the reactivation of HIV-1 replication[48]. These inhibitory effects on viral infection could be explained by the AHR–TIPARP-dependent regulatory mechanism, as viral MAMPs derived from FluV, human cytomegalovirus and HIV-1 have been reported to activate the RIG-I- or the TBK1-interferon pathway in certain cell types[43,49,50]. However, a large number of studies have shown regulatory roles for the AHR not only in xenobiotic detoxification but also in cell proliferation and tumorigenesis[4], and type I interferons are pleiotropic cytokines with antiviral, antitumor and immunomodulatory properties. It will therefore be interesting to investigate the relevance of the AHR–TIPARP-dependent interferon regulation to oncogenesis, tumor progression and immune surveillance.

Collectively, our results provide an association between endogenously activated AHR signaling and innate-sensor-mediated interferon response, which is coupled by TIPARP. Taking also into account the other regulatory roles of endogenous AHR signaling in the adaptive immunity[7–9], pharmacological modification of AHR or TIPARP activity would, therefore, serve as a rational clinical approach for the control of viral infection, inflammation, cancer and, possibly, other diseases.

METHODS

Methods and any associated references are available in the online version of the paper.

Note: Any Supplementary Information and Source Data files are available in the online version of the paper.

Reprints and permissions information is available online at http://www.nature.com/reprints/index.html.

1.   Lindén, J., Lensu, S., Tuomisto, J. & Pohjanvirta, R. Dioxins, the aryl hydrocarbon receptor and the central regulation of energy balance. *Front. Neuroendocrinol.* **31**, 452–478 (2010).

2.   Denison, M.S. & Nagy, S.R. Activation of the aryl hydrocarbon receptor by structurally diverse exogenous and endogenous chemicals. *Annu. Rev. Pharmacol. Toxicol.* **43**, 309–334 (2003).

3.   Hu, W., Sorrentino, C., Denison, M.S., Kolaja, K. & Fielden, M.R. Induction of *Cyp1a1* is a nonspecific biomarker of aryl hydrocarbon receptor activation: results of large scale screening of pharmaceuticals and toxicants *in vivo* and *in vitro*. *Mol. Pharmacol.* **71**, 1475–1486 (2007).

4.   Murray, I.A., Patterson, A.D. & Perdew, G.H. Aryl hydrocarbon receptor ligands in cancer: friend and foe. *Nat. Rev. Cancer* **14**, 801–814 (2014).

5.   Diani-Moore, S. *et al.* Identification of the aryl hydrocarbon receptor target gene TiPARP as a mediator of suppression of hepatic gluconeogenesis by 2,3,7,8-tetrachlorodibenzo-*p*-dioxin and of nicotinamide as a corrective agent for this effect. *J. Biol. Chem.* **285**, 38801–38810 (2010).

6.   Ma, Q., Baldwin, K.T., Renzelli, A.J., McDaniel, A. & Dong, L. TCDD-inducible poly(ADP-ribose) polymerase: a novel response to 2,3,7,8-tetrachlorodibenzo-*p*-dioxin. *Biochem. Biophys. Res. Commun.* **289**, 499–506 (2001).

7.   Nguyen, N.T., Hanieh, H., Nakahama, T. & Kishimoto, T. The roles of aryl hydrocarbon receptor in immune responses. *Int. Immunol.* **25**, 335–343 (2013).

8.   Opitz, C.A. *et al.* An endogenous tumour-promoting ligand of the human aryl hydrocarbon receptor. *Nature* **478**, 197–203 (2011).

9.   Stockinger, B., Di Meglio, P., Gialitakis, M. & Duarte, J.H. The aryl hydrocarbon receptor: multitasking in the immune system. *Annu. Rev. Immunol.* **32**, 403–432 (2014).

10. Moura-Alves, P. *et al.* AhR sensing of bacterial pigments regulates antibacterial defence. *Nature* **512**, 387–392 (2014).

11. Hao, N. & Whitelaw, M.L. The emerging roles of AhR in physiology and immunity. *Biochem. Pharmacol.* **86**, 561–570 (2013).

12. Quintana, F.J. *et al.* Control of T_{reg} and T_H17 cell differentiation by the aryl hydrocarbon receptor. *Nature* **453**, 65–71 (2008).

13. Fernandez-Salguero, P. *et al.* Immune system impairment and hepatic fibrosis in mice lacking the dioxin-binding Ah receptor. *Science* **268**, 722–726 (1995).

14. Benedict, J.C., Lin, T.M., Loeffler, I.K., Peterson, R.E. & Flaws, J.A. Physiological role of the aryl hydrocarbon receptor in mouse ovary development. *Toxicol. Sci.* **56**, 382–388 (2000).

15. Nguyen, L.P. & Bradfield, C.A. The search for endogenous activators of the aryl hydrocarbon receptor. *Chem. Res. Toxicol.* **21**, 102–116 (2008).

16. Gandhi, R. *et al.* Activation of the aryl hydrocarbon receptor induces human type 1 regulatory T cell-like and Foxp3^{+} regulatory T cells. *Nat. Immunol.* **11**, 846–853 (2010).

17. Kimura, A. *et al.* Aryl hydrocarbon receptor in combination with Stat1 regulates LPS-induced inflammatory responses. *J. Exp. Med.* **206**, 2027–2035 (2009).

18. Funatake, C.J., Marshall, N.B., Steppan, L.B., Mourich, D.V. & Kerkvliet, N.I. Cutting edge: activation of the aryl hydrocarbon receptor by 2,3,7,8-tetrachlorodibenzo-*p*-dioxin generates a population of CD4^{+} CD25^{+} cells with characteristics of regulatory T cells. *J. Immunol.* **175**, 4184–4188 (2005).

19. Quintana, F.J. *et al.* An endogenous aryl hydrocarbon receptor ligand acts on dendritic cells and T cells to suppress experimental autoimmune encephalomyelitis. *Proc. Natl. Acad. Sci. USA* **107**, 20768–20773 (2010).

20. Veldhoen, M., Hirota, K., Christensen, J., O'Garra, A. & Stockinger, B. Natural agonists for aryl hydrocarbon receptor in culture medium are essential for optimal differentiation of T_H17 T cells. *J. Exp. Med.* **206**, 43–49 (2009).

21. Veldhoen, M. *et al.* The aryl hydrocarbon receptor links T_H17-cell-mediated autoimmunity to environmental toxins. *Nature* **453**, 106–109 (2008).

22. Vorderstrasse, B.A., Bohn, A.A. & Lawrence, B.P. Examining the relationship between impaired host resistance and altered immune function in mice treated with TCDD. *Toxicology* **188**, 15–28 (2003).

23. Warren, T.K., Mitchell, K.A. & Lawrence, B.P. Exposure to 2,3,7,8-tetrachlorodibenzo-*p*-dioxin (TCDD) suppresses the humoral and cell-mediated immune responses to influenza A virus without affecting cytolytic activity in the lung. *Toxicol. Sci.* **56**, 114–123 (2000).

24. Jin, G.B., Winans, B., Martin, K.C. & Lawrence, B.P. New insights into the role of the aryl hydrocarbon receptor in the function of CD11c^{+} cells during respiratory viral infection. *Eur. J. Immunol.* **44**, 1685–1698 (2014).

25. Wheeler, J.L., Martin, K.C., Resseguie, E. & Lawrence, B.P. Differential consequences of two distinct AhR ligands on innate and adaptive immune responses to influenza A virus. *Toxicol. Sci.* **137**, 324–334 (2014).

26. Stone, T.W., Stoy, N. & Darlington, L.G. An expanding range of targets for kynurenine metabolites of tryptophan. *Trends Pharmacol. Sci.* **34**, 136–143 (2013).

27. Honda, K., Takaoka, A. & Taniguchi, T. Type I interferon gene induction by the interferon regulatory factor family of transcription factors. *Immunity* **25**, 349–360 (2006).

28. Chi, H. & Flavell, R.A. Innate recognition of non-self nucleic acids. *Genome Biol.* **9**, 211 (2008).

29. Goubau, D., Deddouche, S. & Reis e Sousa, C. Cytosolic sensing of viruses. *Immunity* **38**, 855–869 (2013).

30. Medzhitov, R. Recognition of microorganisms and activation of the immune response. *Nature* **449**, 819–826 (2007).

31. Takeuchi, O. & Akira, S. Pattern recognition receptors and inflammation. *Cell* **140**, 805–820 (2010).

32. Rehwinkel, J. & Reis e Sousa, C. RIGorous detection: exposing virus through RNA sensing. *Science* **327**, 284–286 (2010).

33. Sato, S. *et al.* The RNA sensor RIG-I dually functions as an innate sensor and direct antiviral factor for hepatitis B virus. *Immunity* **42**, 123–132 (2015).

34. Weber, M. & Weber, F. Segmented negative-strand RNA viruses and RIG-I: divide (your genome) and rule. *Curr. Opin. Microbiol.* **20**, 96–102 (2014).

35. Yoneyama, M. *et al.* The RNA helicase RIG-I has an essential function in double-stranded RNA-induced innate antiviral responses. *Nat. Immunol.* **5**, 730–737 (2004).

36. Sun, L., Wu, J., Du, F., Chen, X. & Chen, Z.J. Cyclic GMP-AMP synthase is a cytosolic DNA sensor that activates the type I interferon pathway. *Science* **339**, 786–791 (2013).

37. Kim, S.H. *et al.* Novel compound 2-methyl-2H-pyrazole-3-carboxylic acid (2-methyl-4-*o*-tolylazo-phenyl)-amide (CH-223191) prevents 2,3,7,8-TCDD-induced toxicity by antagonizing the aryl hydrocarbon receptor. *Mol. Pharmacol.* **69**, 1871–1878 (2006).

38. Madge, D.J. *et al.* Novel tryptophan dioxygenase inhibitors and combined tryptophan dioxygenase/5-HT reuptake inhibitors. *Bioorg. Med. Chem. Lett.* **6**, 857–860 (1996).

39. Ahmed, S. *et al.* Loss of the mono-ADP-ribosyltransferase, Tiparp, increases Sensitivity to dioxin-induced steatohepatitis and lethality. *J. Biol. Chem.* **290**, 16824–16840 (2015).

40. MacPherson, L. *et al.* 2,3,7,8-tetrachlorodibenzo-*p*-dioxin poly(ADP-ribose) polymerase (TiPARP, ARTD14) is a mono-ADP-ribosyltransferase and repressor of aryl hydrocarbon receptor transactivation. *Nucleic Acids Res.* **41**, 1604–1621 (2013).

41. Hayakawa, S. *et al.* ZAPS is a potent stimulator of signaling mediated by the RNA helicase RIG-I during antiviral responses. *Nat. Immunol.* **12**, 37–44 (2011).

42. Schreiber, V., Dantzer, F., Ame, J.C. & de Murcia, G. Poly(ADP-ribose): novel functions for an old molecule. *Nat. Rev. Mol. Cell Biol.* **7**, 517–528 (2006).

43.   Kato, H. *et al.* Differential roles of MDA5 and RIG-I helicases in the recognition of RNA viruses. *Nature* **441**, 101–105 (2006).

44.   Kubota, T. *et al.* Virus infection triggers SUMOylation of IRF3 and IRF7, leading to the negative regulation of type I interferon gene expression. *J. Biol. Chem.* **283**, 25660–25670 (2008).

45.   Ma, X. *et al.* Molecular basis of Tank-binding kinase 1 activation by transautophosphorylation. *Proc. Natl. Acad. Sci. USA* **109**, 9378–9383 (2012).

46.   Zhao, W. Negative regulation of TBK1-mediated antiviral immunity. *FEBS Lett.* **587**, 542–548 (2013).

47.   Murayama, T., Inoue, M., Nomura, T., Mori, S. & Eizuru, Y. 2,3,7,8-tetrachlorodibenzo-*p*-dioxin is a possible activator of human cytomegalovirus replication in a human fibroblast cell line. *Biochem. Biophys. Res. Commun.* **296**, 651–656 (2002).

48.   Ohata, H., Tetsuka, T., Hayashi, H., Onozaki, K. & Okamoto, T. 3-Methylcholanthrene activates human immunodeficiency virus type 1 replication via aryl hydrocarbon receptor. *Microbiol. Immunol.* **47**, 363–370 (2003).

49.   Berg, R.K. *et al.* Genomic HIV RNA induces innate immune responses through RIG-I-dependent sensing of secondary-structured RNA. *PLoS One* **7**, e29291 (2012).

50.   Gravel, S.P. & Servant, M.J. Roles of an IκB kinase-related pathway in human cytomegalovirus-infected vascular smooth muscle cells: a molecular link in pathogen-induced proatherosclerotic conditions. *J. Biol. Chem.* **280**, 7477–7486 (2005).

Ed summary:

The aryl hydrocarbon receptor (AHR) has well-described roles in the differentiation of T cells; however, less is known about its function in innate immunity. Takaoka and colleagues demonstrate how an AHR-dependent pathway reins in production of type I interferon.

Figure 1 Endogenously activated AHR signaling modulates IFN-I-mediated antiviral response. (**a**) IFN-β production by infection with various viruses for 24 h in wild-type ($Ahr^{+/+}$) and $Ahr^{-/-}$ MEFs. $n = 3$ samples per group. (**b**) Viral titers after 24 h of infection with VSV or FluV in $Ahr^{+/+}$ or $Ahr^{-/-}$ MEFs. PFU, plaque-forming units; $n = 3$ samples per group. (**c**) IFN-β production 24 h after FluV infection in $Ahr^{+/+}$ or $Ahr^{-/-}$ BMDMs. $n = 3$ samples per group. (**d**) ELISA of IFN-β (left) and plaque-forming assay of viral titers (right) in bronchoalveolar lavage fluid (BALF) from $Ahr^{+/+}$ and $Ahr^{-/-}$ mice infected intranasally for 36 h with FluV. Horizontal bars represent mean values. $n = 9$ mice per group. (**e**) Concentration of IFN-β measured by ELISA in wild-type MEFs pretreated with CH-223191 (3 μM) or DMSO (negative control) for 48 h and infected with VSV or stimulated with 3pRNA or cGAMP for 24 h. $n = 3$ samples per group. *$P < 0.05$, **$P < 0.01$ (Student's t-test). Data are representative of at least two independent experiments (mean ± s.d.). ND, not detected.

Figure 2 AHR activation by endogenous ligands suppresses virus-induced IFN-I response. (**a**) Quantitative RT-PCR analysis of *Ifnb1* induction after 3pRNA stimulation in MEFs pretreated with control (C; PBS for Kyn, DMSO for FICZ), Kyn (50, 100 or 200 μM) or FICZ (0.1, 1 and 25 nM). Data are normalized to expression of *Actb* mRNA. $n = 3$ samples per group. (**b**) IFN-β production after infection with various viruses for 24 h in MEFs pretreated with PBS (negative control) or Kyn (200 μM) or DMSO (negative control) or FICZ (25 nM) for 2 h. $n = 3$ samples per group. (**c**) ELISA of IFN-β response by VSV infection in $Ahr^{+/+}$ and $Ahr^{-/-}$ MEFs pretreated with 680C91 or not pretreated (DMSO). $n = 3$ samples per group. (**d**) ELISA of IFN-β (left) and plaque-forming assay of viral titers (right) in sera from $Ahr^{+/+}$ and $Ahr^{-/-}$ mice infected i.p. for 36 h with VSV after i.p. injection with corn oil (–) or FICZ (2 μg per mouse). Horizontal lines indicate mean values. $n = 7$ mice per group. *$P < 0.05$, **$P < 0.01$ (Student's t-test). Data are representative of at least two independent experiments (mean ± s.d.) ND, not detected; NS, not significant; PFU, plaque-forming units.

Figure 3 TIPARP is a responsible factor for AHR-mediated downregulation of IFN-I induction. (**a**) Quantitative RT-PCR analysis of 3pRNA-induced *Ifnb1* mRNA expression in Kyn-treated MEFs after transfection with siRNAs against (si-) various gene products. (**b**) Quantitative RT-PCR analysis of *Tiparp* mRNA in MEFs treated with Kyn (50, 100 or 200 μM) or FICZ (0.1, 1 or 25 nM) for 2 h. (**c**) Quantitative RT-PCR analysis of *Tiparp*

mRNA expression in $Ahr^{+/+}$ or $Ahr^{-/-}$ MEFs treated with Kyn or FICZ for 2 h. Data are normalized to the expression of *Actb* mRNA for each sample; $n = 3$ samples per group (**a**–**c**). (**d**) IFN-β production after NDV infection for 24 h in HEK293T cells expressing control plasmid or TIPARP. $n = 3$ samples per group. (**e**) IFN-β production after 3pRNA stimulation in HEK293T cells cotransfected with empty vector (C) or mouse TIPARP (T) expression vector and control siRNA (siControl) or two different siRNA against TIPARP (siTIPARP-1 and siTIPARP-2). $n = 3$ samples per group. $*P < 0.05$, $**P < 0.01$ (Student's *t*-test). Data are representative of at least two independent experiments with similar results (mean ± s.d.).

Figure 4 TIPARP deficiency robustly induces IFN-I response to viral infection. (**a**) Quantitative RT-PCR analysis of *Ifnb1* mRNA induction in response to viral MAMPs in $Tiparp^{+/+}$ or $Tiparp^{-/-}$ MEFs. Data are normalized to the expression of *Actb* mRNA for each sample. $n = 3$ samples per group. (**b**) IFN-β production by 3pRNA or cGAMP in $Tiparp^{+/+}$ or $Tiparp^{-/-}$ MEFs analyzed by ELISA. $n = 3$ samples per group. (**c**) Quantitative RT-PCR analysis of *Ifnb1* mRNA induction after viral infection of $Tiparp^{+/+}$ or $Tiparp^{-/-}$ MEFs. $n = 3$ samples per group. (**d**) Quantitative RT-PCR analysis (left) or ELISA (right) of IFN-β response in $Tiparp^{+/+}$ or $Tiparp^{-/-}$ MEFs after 6 h or 24 h of NDV infection, respectively. *Ifnb1* mRNA data are normalized to the expression of *Actb* mRNA for each sample. $n = 3$ samples per group. (**e**) IFN-β production by FluV infection in $Tiparp^{+/+}$ or $Tiparp^{-/-}$ BMDMs analyzed by ELISA. $n = 3$ samples per group. (**f**) Plaque-forming assay of viral titers after 24 h of infection with the indicated viruses in $Tiparp^{+/+}$ or $Tiparp^{-/-}$ MEFs. $n = 3$ samples per group. $*P < 0.05$, $**P < 0.01$ (Student's *t*-test). Data are representative of at least two independent experiments with similar results (mean ± s.d.). ND, not detected; PFU, plaque-forming units.

Figure 5 TIPARP regulates TBK1 activity via its post-translational modification. (**a**) Luciferase activity of a p-125Luc (*IFNB1* promoter) reporter plasmid in HEK293T cells transfected with expression vectors for various proteins along with a control or TIPARP expression vector. Data are normalized to the activity of Renilla luciferase. $n = 3$ samples per group. N-RIG, N-terminal RIG-I. (**b**) Native PAGE and SDS-PAGE and immunoblot (IB) analysis of TBK1-induced dimerization of endogenous IRF-3 in $Tiparp^{+/+}$ or $Tiparp^{-/-}$ MEFs and band intensity of the IRF-3 dimer relative to that of the IRF-3 monomer, assessed by densitometry. (**c**) Immunoprecipitation of endogenous TIPARP

18

and TBK1 in HEK293T after 4 h of 3pRNA stimulation (10 μg/ml) (top) and band intensity of associated TBK1 relative to that of immunoprecipitated TIPARP, assessed by densitometry (bottom). WCL, whole cell lysate. (**d**) Colocalization of YFP-tagged TIPARP and TBK1 (Alexa Fluor 594) in HeLa cells unstimulated or after 4 h of 3pRNA stimulation. Nuclei were counterstained with Hoechst 33342. Scale bars, 10 μm. High magnification images are shown as insets. (**e**) Immunoblot analysis of phosphorylated TBK1 (TBK1(pS172) and IRF-3 (IRF-3(pS396)) in *Tiparp*$^{+/+}$ or *Tiparp*$^{-/-}$ MEFs infected with VSV. (**f**) Autoradiographic analysis of ADP-ribosylated recombinant TBK1 (rTBK1) after incubation with rGST-TIPARP(WT) or rGST-TIPARP(H532A) in the presence of [^{32}P]NAD$^+$. β-NAD$^+$ was added as a cold competitor. (**g**) Immunoblot analysis of ADP-ribosylated TBK1 in *Tiparp*$^{+/+}$ or *Tiparp*$^{-/-}$ MEFs infected with VSV for 8 h. (**h**) Immunoblot analysis of autophosphorylated rTBK1 after incubation with rGST-TIPARP(WT) or rGST-TIPARP(H532A). (**i**) IFN-β production (left) and viral titers (right) after FluV infection for 36 h in *Tiparp*$^{-/-}$ MEFs transfected with a TIPARP(WT) or TIPARP(H532A) expression vector. $n = 3$ samples per group. **P < 0.01 (Student's *t*-test). Data are representative of at least two independent experiments with similar results. NS, not significant; PFU, plaque-forming units.

Figure 6 Constitutive activation of the AHR-TIPARP axis modulates interferon-mediated antiviral innate defense. (**a**) Quantitative RT-PCR analysis of *Ifnb1* mRNA induction by 3pRNA stimulation or FluV infection in *Tiparp*$^{+/+}$ or *Tiparp*$^{-/-}$ MEFs with or without pretreatment with Kyn (200 μM) or FICZ (25 nM). Data are shown as the percentage of control (3pRNA or FluV-induced *Ifnb1* mRNA levels without pretreatment). $n = 3$ samples per group. (**b,c**) IFN-β production (**b**) and plaque-forming assay to determine viral titers (**c**) after FluV infection for 24 h in wild-type (WT), *Ahr*$^{-/-}$ or *Tiparp*$^{-/-}$ MEFs pretreated with CH-223191 (3 μM) or vehicle (DMSO). $n = 3$ samples per group. (**d**) ELISA of IFN-β (left) and plaque-forming assay of viral titers (right) in BALF from WT mice infected intranasally for 36 h with FluV after i.p. injection with corn oil (control) or CH-223191 (100 μg per mouse). Horizontal bars indicate mean values. $n = 8$ mice per group. (**e**) Survival rates of C57BL/6N mice intranasally infected with FluV after i.p. administration of corn oil (control) or CH-223191. $n = 5$ mice per group. *P* = 0.0175. (**f**) ELISA of IFN-β in BALF from littermate WT and *Tiparp*$^{-/-}$ mice infected intranasally for 36 h with FluV after i.p. injection with corn oil (–) or CH-223191.

Horizontal bars indicate mean values. $n = 4$ mice per group. $**P < 0.01$, Student's t-test (**a**–**d**,**f**) or log-rank test (**e**). Data are representative of at least two independent experiments with similar results (mean ± s.d.). NS, not significant. ND, not detected; PFU, plaque-forming units.

ONLINE METHODS

Cells, antibodies and reagents. $Ahr^{+/+}$ and $Ahr^{-/-}$ MEFs were from C.A. Bradfield[51] and were grown in DMEM with 10% heat-inactivated FBS. BMDMs were derived from $Ahr^{-/-}$ mice[52] (provided by A. Kimura and Y. Fujii-Kuriyama) or $Tiparp^{-/-}$ mice[53]. Immortalized $Tiparp^{+/+}$ and $Tiparp^{-/-}$ MEFs were previously established[40]. HEK293T and HeLa cells were purchased from American Type Culture Collection and cultured as described[41,54]. Human primary CD14$^+$ monocytes (>95% CD14$^+$ as determined by flow cytometry) were obtained from peripheral blood mononuclear cells (PBMCs) of healthy volunteer donor-derived whole blood by magnetic-activated cell sorting with magnetic microbeads according to the manufacturer's instructions (Miltenyi Biotec). Experiments with human whole blood (provided by Japan Red Cross Society, who obtained informed consent from blood donors) were approved by the institutional review board of Hokkaido University. Sf9 cells were purchased from Invitrogen and routinely grown at 28 °C in a Sf-900 II SFM medium (Gibco) supplemented with 5% heat-inactivated FBS and 25 ng/ml gentamycin (Gibco). These cell lines were tested for mycoplasma contamination by staining (DAPI) or nested PCR. Antibodies were used as follows: anti-Flag (M2; Sigma), anti-hemagglutinin (5D8; MBL, 3F10; Roche), anti-GST (B-14; Santa Cruz), anti-IRF3 (IRF35I218-2; MBR, FL-425; Santa Cruz, 51-3200; Invitrogen), anti-IRF3(pS396) (4D4G; Cell Signaling), anti-TBK1 (EP611Y; Abcam), anti-TBK1(pS172) (D52C2; Cell Signaling, J133-1171; BD Pharmingen), anti-TIPARP (SAB2102431; Sigma), anti-nucleoporin p62 (51-9002029; BD Biosciences), anti-α-tubulin (DM1A; Cell Signaling) and anti-β-actin (AC-15; Sigma). Working dilutions of antibodies for immunoblotting were as follows: anti-Flag (M2), 1:1,000; anti-hemagglutinin (3F10), 0.5 μg/ml; anti-GST (B-14), 1:1,000; anti-IRF3 (IRF35I218-2), 1:1,000; anti-IRF3 (FL-425), 1:100; anti-IRF3 (51-3200), 0.5 μg/ml; anti-IRF3(pS396) (4D4G), 1:1,000; anti-TBK1 (EP611Y), 1:1,000; anti-TBK1(pS172) (D52C2), 1:1,000; anti-TBK1(pS172) (J133-1171), 1:500; anti-TIPARP (SAB2102431), 0.5 μg/ml; anti-nucleoporin p62 (51-9002029), 1:1,000, anti-α-tubulin (DM1A), 1:1,000;

anti-β-actin (AC-15), 1:1,000. L-Kyn and FICZ were from Sigma and Enzo Life Sciences, respectively. L-Trp-free DMEM was from Cell Science and Technology Institute. The 3pRNA and dsVACV 70-mer oligonucleotides were prepared as reported[41,55]. Poly(rI:rC) and cGAMP were purchased from GE Healthcare and Biolog, respectively. Cycloheximide (CHX), CH-223191, 680C91, 1-methyl-L-tryptophan (1-MT) and human recombinant IL-1β were purchased from Sigma. Leptomycin B was purchased from Enzo Life Sciences. Lipofectamine 2000 and Lipofectamine RNAiMAX (Invitrogen) were used for transfection of nucleic acid ligands into the cytoplasm. FuGENE6 (Roche) reagent was used for gene transfer with lipid transfection.

Plasmids and molecular cloning. The cDNAs for human TIPARP, N-terminal RIG-I, MAVS, TBK1, mouse TIPARP and the related mutants of TIPARP and TBK1 (ref. 56) were obtained by RT-PCR of total RNAs from HeLa or HEK293T cells or MEFs. The cDNA was then cloned into a pTA2 vector with the Target Clone-Plus-TA cloning kit (Toyobo). For YFP-, Flag- and HA-tagged proteins, cDNA was cloned into the XhoI and NotI sites of the pCAGGS-YFP, pCXN2-Flag or pIRM-3HA vector. For mCherry-tagged TBK1 protein, the cDNA of TBK1 was cloned into the BglII and SacII sites of the pmCherry-C1 vector (Clontech). The nucleotide sequence of each cDNA was confirmed with the BigDye Terminator v3.1 sequencing kit (Applied Biosystems). The vectors pCAGGS and Venus (called YFP here) were provided by J. Miyazaki and A. Miyawaki, respectively. The expression vector for the constitutive active form of IRF-3, pcDNA3.1(-)IRF-3/5D-FLAG was provided by T. Kubota[44]. For the generation of expression plasmids for recombinant proteins, the cDNAs encoding glutathione *S*-transferase (GST), GST-TIPARP(WT), GST-TIPARP(H532A) and GST-TBK1 (WT, KD, or ULD+CC) were cloned into BamHI and HindIII sites of the pFastBac1 vector (Invitrogen).

qRT-PCR analysis. Total RNAs were isolated from culture cells or mouse organs using Isogen (Nippon Gene) and were treated with DNase I (Invitrogen). cDNAs were prepared from total RNAs using ReverTra Ace (Toyobo). qPCR was performed using SYBR Premix Ex Taq (Takara) and analyzed on a StepOnePlus real-time PCR system (Applied Biosystems). Detailed information about the primers used is shown in **Supplementary Table 1**. Data were normalized to the expression levels of *ACTB* or *GAPDH* for each sample.

Viral infection in cells and measurement of viral titers. Wild-type, $Ahr^{-/-}$ or $Tiparp^{-/-}$ MEFs were infected with VSV (New Jersey strain, 0.1 multiplicity of infection (m.o.i.)), FluV (A/Puerto Rico/8/1934 H1N1 strain, 0.1 m.o.i.), NDV (LaSota strain, 80 hemagglutination units (HAU) per 2×10^5 cells), SeV (200 HAU per 2×10^5 cells), EMCV (1 m.o.i.) or HSV-1 (1 m.o.i.). Cells were infected for 1 h at 37 °C in serum-free MEM containing amino acids and trypsin (for FluV), or in serum-free DMEM (for NDV, VSV, SeV and HSV-1). BMDMs were infected for 1 h at 37 °C with FluV in serum-free MEM containing amino acids and trypsin. Plaque-forming assays with Madin–Darby canine kidney cells were conducted to measure the titers of FluV. Vero cells were used for plaque-forming assays to determine the titers of VSV, EMCV and HSV-1.

ELISA. Human and murine IFN-α/β proteins in 24-h culture supernatants, sera from mice at 12 h after infection with VSV or bronchoalveolar lavage fluid (BALF) from mice at 36 h after infection with FluV were measured by ELISA according to the manufacturer's protocol (PBL).

AHR ligands and their treatments. For Kyn or FICZ treatment, MEFs were precultured in L-Trp-free DMEM with 10% heat-inactivated and dialyzed FBS[8]. At 24 h after the absence of L-Trp, cells were treated with Kyn or FICZ for 2 h and subjected to further experiment.

FICZ exposure and viral infection *in vivo*. C57BL/6NJcl mice were obtained from CLEA Japan. $Ahr^{-/-}$ C57BL/6N mice were purchased from Taconic. FICZ was dissolved in corn oil (Sigma) to 10 mg/ml. Mice were injected i.p. with FICZ (2 mg per mouse). Twelve hours later, mice were i.p. infected with VSV (Indiana strain, 3×10^8 PFU per mouse). Female mice (6 weeks of age) were used for the experiments. These animal experiments were approved by the Committee for Animal Research at Hokkaido University and were performed according to the Hokkaido University Manual for Implementing Animal Experimentation.

Cycloheximide (CHX) treatment. 2×10^5 MEFs were seeded on 12-well plates and pretreated with 10 μg/ml CHX in DMEM for 1 h.

siRNA-mediated gene silencing. Chemically synthesized 21-nucleotide siRNAs, including control siRNA (siPerfect Negative Control), were obtained from Sigma or Hokkaido system science (sequence information is given in **Supplementary Table 2**).

MEFs and HEK293T cells were transfected with 50 nM siRNA in 2.0 µl Lipofectamine 2000 or Lipofectamine RNAiMAX. At 48 h after transfection, the cells were used for further experiments.

Luciferase assay. In **Figure 5a**, HEK293T cells seeded on 24-well plates were cotransfected with 100 ng of p-125Luc luciferase reporter plasmid (provided by T. Fujita) together with the increasing doses of TIPARP expression vector (0.01, 0.1, and 1 µg) or together with 200 ng of the expression vectors (N-RIG-I, MAVS, TBK1 or IRF-3/5D) and/or 100 ng of TIPARP expression vector. In **Supplementary Figure 3b**, at 24 h after transfection, cells were stimulated with 3pRNA (1 µg/ml) for 24 h. Luciferase activity was measured with the Dual-Luciferase Reporter Assay system (Promega). The Renilla luciferase reporter plasmid (10 ng) was used as an internal control.

Immunoprecipitation and immunoblotting. Cell lysis, immunoblot analysis and immunoprecipitation assays were done as described[41,54]. For the detection of endogenous IRF-3 dimer, wild-type or *Tiparp*^{−/−} MEFs seeded on 6-well plates were transfected with control or mouse TBK1 expression vector (3 µg), and IRF-3 dimer formation was assessed 48 h later by native PAGE followed by immunoblot analysis as described[41].

Fluorescence analysis. HeLa cells transfected with 1.0 µg of the YFP-tagged TIPARP expression vector were stimulated with 3pRNA for 4 h. Endogenous TBK1 was visualized with anti-TBK1 (dilution, 1:500) and the appropriate secondary antibody conjugated to Alexa Fluor 594 (Molecular Probes) (10 µg/ml). Hoechst 33342 (Invitrogen) was used for the counterstaining of nuclei. The localization of TIPARP and TBK1 was examined with an IX-81S confocal microscope (Olympus). For FRET analysis, HeLa cells were transfected with both YFP-tagged TIPARP and mCherry-tagged TBK1 expression vector, and then FRET analysis was performed with IX81 fluorescence microscope (Olympus). We used the following filters in this study: BP490-500HQ (Olympus) and FF01-542/27-25 (Semrock) excitation/emission filters for the YFP images; BP535-555HQ and BA570-625HQ (Olympus) for mCherry; and BP490-500HQ and BP590 for FRET. As a dichroic mirror, a DM505HQ glass reflector (Olympus) was used. $FRET^c = FRET - 0.1041 \times YFP - 0.0199 \times mCherry$, where FRET, YFP and mCherry indicate fluorescence intensities acquired for the FRET, YFP and RFP channels, respectively, with the background fluorescence intensity subtracted. FRET efficiency was calculated as a quotient of background-subtracted FRET and YFP images,

and was presented in an intensity-modified display mode with MetaMorph software. In the intensity-modified display mode shown in **Supplementary Fig. 4b**, eight colors from red to blue are used to represent the emission ratio, with the intensity of each color.

Nuclear–cytosolic protein fractionation. 6×10^5 cells of HEK293T cells were seeded on 6-well plates and transfected with 1.0 μg HA-tagged TIPARP expression vector. Twenty-four hours later, these cells were pretreated with leptomycin B (200 μg/ml) for 2 h then stimulated with 3pRNA (10 μg/ml) for 4 h. Nuclear–cytosolic protein fractionation was performed according to the manufacturer's protocol (CelLytic NuCLEAR Extraction Kit; Sigma).

Purification of recombinant proteins. GST and GST-tagged TBK1 (WT, KD, or ULD+CC), TIPARP and TIPARP(H532A) were expressed in Sf9 cells according to the manufacturer's instructions for Bac-to-Bac baculovirus expression system (Invitrogen) and purified with glutathione Sepharose 4B (GE Healthcare). GST protein of recombinant GST-TBK1 was cleaved with Precision protease (GE Healthcare).

***In vitro* ADP-ribosylation assay and *in vitro* kinase assay.** For *in vitro* ADP-ribosylation assay, purified recombinant TBK1 (10 ng) was incubated with GST-tagged TIPARP(WT) or TIPARP(H532A) (2,500 ng each) at 30 °C in 30 μl PARP buffer (50 mM Tris-HCl (pH 8.0), 0.2 mM DTT, 4 mM $MgCl_2$, 0.1 μg/ml BSA) containing 2 μCi $[^{32}P]NAD^+$ (Perkin-Elmer). β-NAD$^+$ (500 μM, Sigma) was added as a competitor. ADP-ribosylated TBK1 was detected by autoradiography after SDS-PAGE. For *in vitro* protein kinase assay, purified recombinant TBK1 (100 ng) was incubated with GST-tagged TIPARP(WT) or TIPARP(H532A) (2,500 ng each) at 30 °C in 30 μl PARP buffer containing β-NAD$^+$ (500 μM), then 12 μl of ADP-ribosylated TBK1 protein was incubated at 30 °C for 15 min in 30 μl reaction mixture containing 50 mM HEPES (pH 8.0), 10 mM $MgCl_2$, 2.5 mM EGTA, 1 mM DTT, 10 mM β-glycerophosphate, 1 mM NaF, 0.1 mM Na_3VO_4, 0.1 mM APMSF, and 1 mM ATP. Phosphorylation of TBK1 was assessed by immunoblot with anti-TBK1(pS172).

Pulldown assay. 5×10^5 cells of wild-type or *Tiparp*$^{-/-}$ MEFs were seed on 6-well plates and incubated in 10% DMEM containing 6-biotin-17-NAD (biotin-NAD; Trevigen) (6 μg/ml) for 24 h. These cells were then, infected with VSV (New Jersey strain, 0.1 m.o.i.) or stimulated with 3pRNA (10 μg/ml) for 8 h. Cell lysates were incubated with

streptavidin-conjugated magnetic beads (Invitrogen) for 30 min at room temperature. The beads were washed and subjected to SDS-PAGE and immunoblot analysis.

CH-223191, 680C91 or 1-MT treatment in cells. 1×10^5 wild-type, *Tiparp*$^{-/-}$ or *Ahr*$^{-/-}$ MEFs were seeded on 12-well plates and pretreated with 3 μM CH-223191 for 48 h or 10 μM 680C91 for 24 h and subjected to further experiment. 2.5×10^5 wild-type BMDMs were seeded on 12-well plates and treated with 200 nM 1-MT for 24 h and subjected to further experiment. CH-223191 is reported to be a specific antagonist of AHR, which does not have detectable AHR agonist-like activity or estrogenic potency[37].

CH-223191 exposure and viral infection *in vivo*. C57BL/6NJcl mice were obtained from CLEA Japan. *Tiparp*$^{-/-}$ mice were described previously[53]. CH-223191 was dissolved in corn oil (Sigma) to 0.5 mg/ml. Mice were exposed to CH-223191 (100 μg per mouse) by i.p. injection. At 4 h after exposure to CH-223191, mice were intranasally infected with FluV (1×10^4 plaque-forming units (PFU) per mouse). Male and female mice (6 weeks of age) were used for the experiments. These animal experiments were approved by the committee reviews of Hokkaido University and University of Toronto.

Measurement of Kyn and Trp concentrations. 1×10^5 wild-type MEFs were seeded on 12-well plates and treated with 10 μM 680C91 for 24 h. 2.5×10^5 wild-type BMDMs were seeded on 12-well plates and treated with 200 nM 1-MT for 24 h. Kyn and Trp concentrations in the culture supernatants were measured by ELISA according to the manufacturer's protocol (Immundiagnostik and LDN, respectively). In the experiments (**Fig. 2c**) that support the role of the constitutive AHR signaling induced by endogenous AHR ligands, the concentration of Kyn in culture medium (without TDO or IDO inhibitors) is approximately 1.54 μM (**Supplementary Fig. 2b,c**), which is almost equivalent to the serum concentration of endogenous Kyn[57] (2.4 ± 0.1 μM).

Statistical analysis. Values are shown as mean ± s.d. Statistical significance between two samples was determined by Student's *t*-test. Kaplan–Meier plots were constructed and a log–rank test was used to test for differences in survival between control and CH-223191-treated mice after FluV infection.

51.   Schmidt, J.V., Su, G.H., Reddy, J.K., Simon, M.C. & Bradfield, C.A. Characterization of a murine *Ahr* null allele: involvement of the Ah receptor in

hepatic growth and development. *Proc. Natl. Acad. Sci. USA* **93**, 6731–6736 (1996).

52. Mimura, J. *et al.* Loss of teratogenic response to 2,3,7,8-tetrachlorodibenzo-*p*-dioxin (TCDD) in mice lacking the Ah (dioxin) receptor. *Genes Cells* **2**, 645–654 (1997).

53. Schmahl, J., Raymond, C.S. & Soriano, P. PDGF signaling specificity is mediated through multiple immediate early genes. *Nat. Genet.* **39**, 52–60 (2007).

54. Takaoka, A. *et al.* DAI (DLM-1/ZBP1) is a cytosolic DNA sensor and an activator of innate immune response. *Nature* **448**, 501–505 (2007).

55. Unterholzner, L. *et al.* IFI16 is an innate immune sensor for intracellular DNA. *Nat. Immunol.* **11**, 997–1004 (2010).

56. Cui, J. *et al.* NLRP4 negatively regulates type I interferon signaling by targeting the kinase TBK1 for degradation via the ubiquitin ligase DTX4. *Nat. Immunol.* **13**, 387–395 (2012).

57. Laich, A., Neurauter, G., Widner, B. & Fuchs, D. More rapid method for simultaneous measurement of tryptophan and kynurenine by HPLC. *Clin. Chem.* **48**, 579–581 (2002).
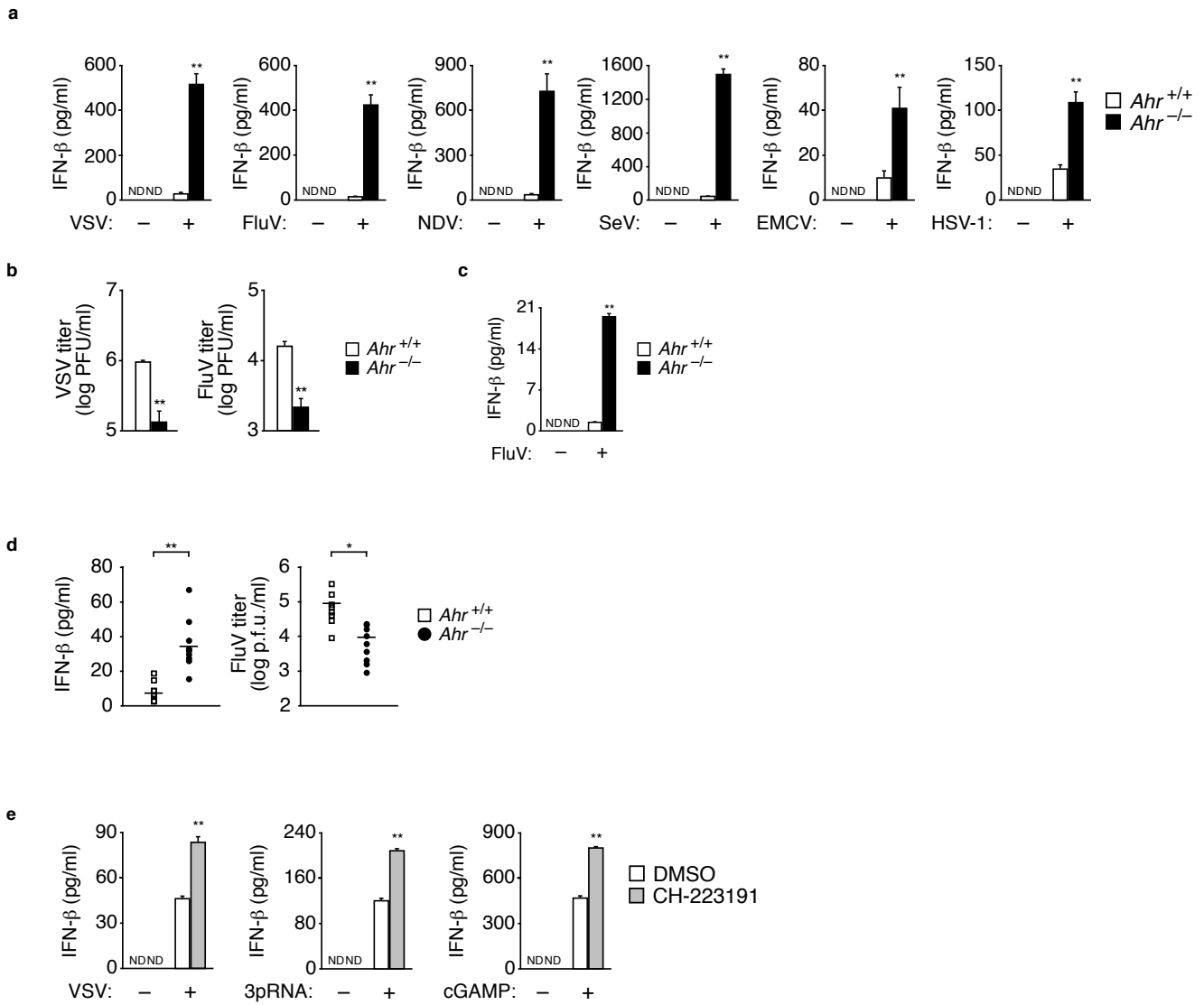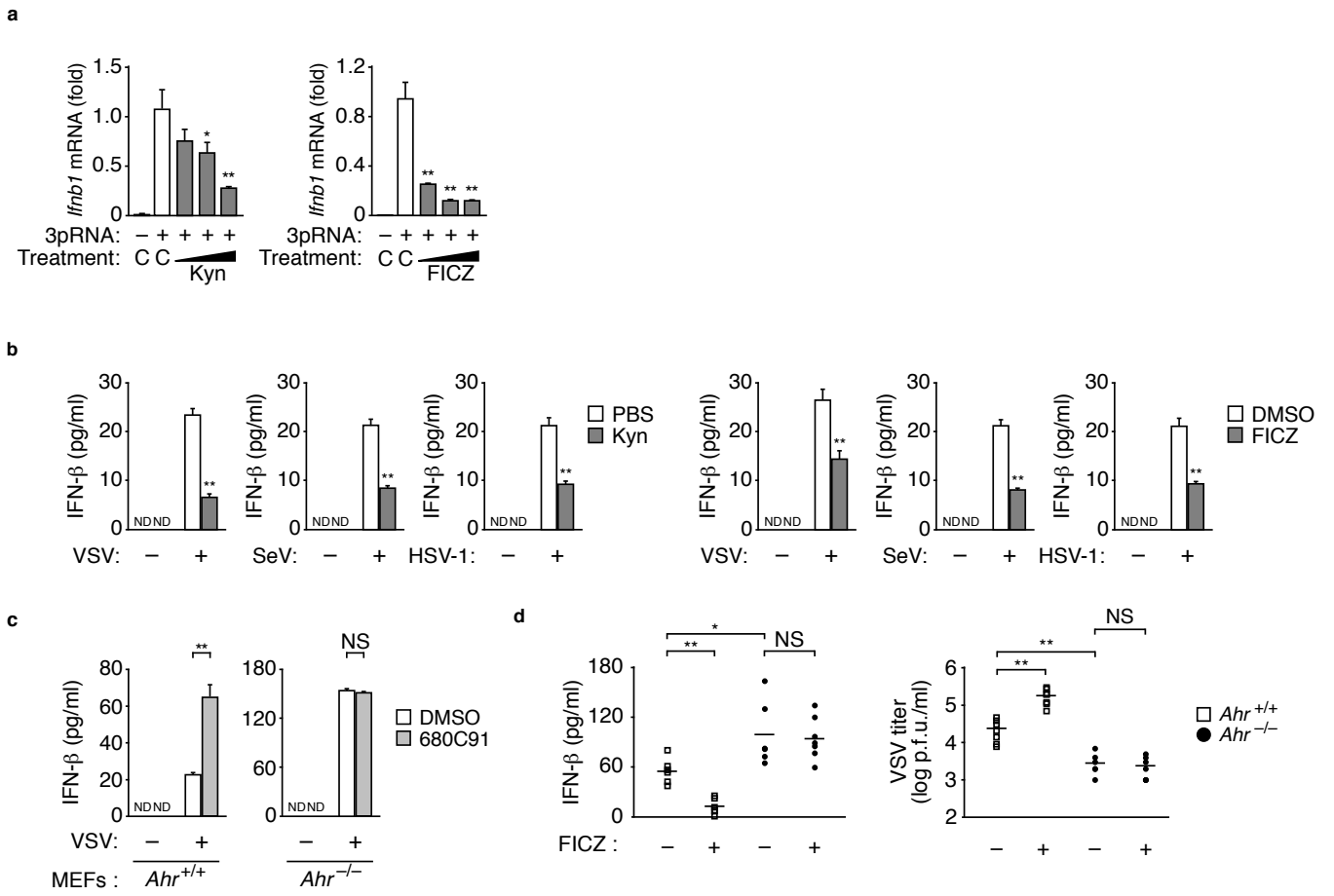
Figure 1 Yamada *et al*.

a

b

c

d

e

Figure 2 Yamada *et al*.

a

b
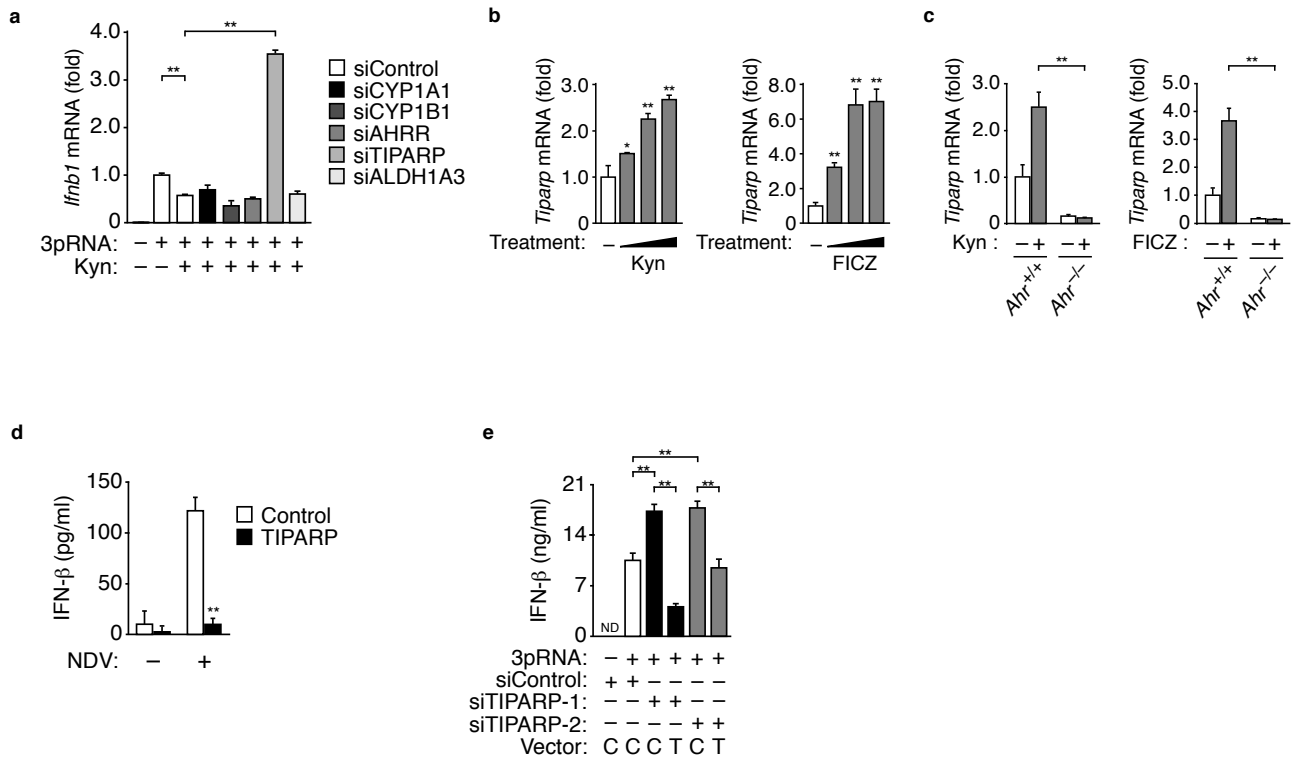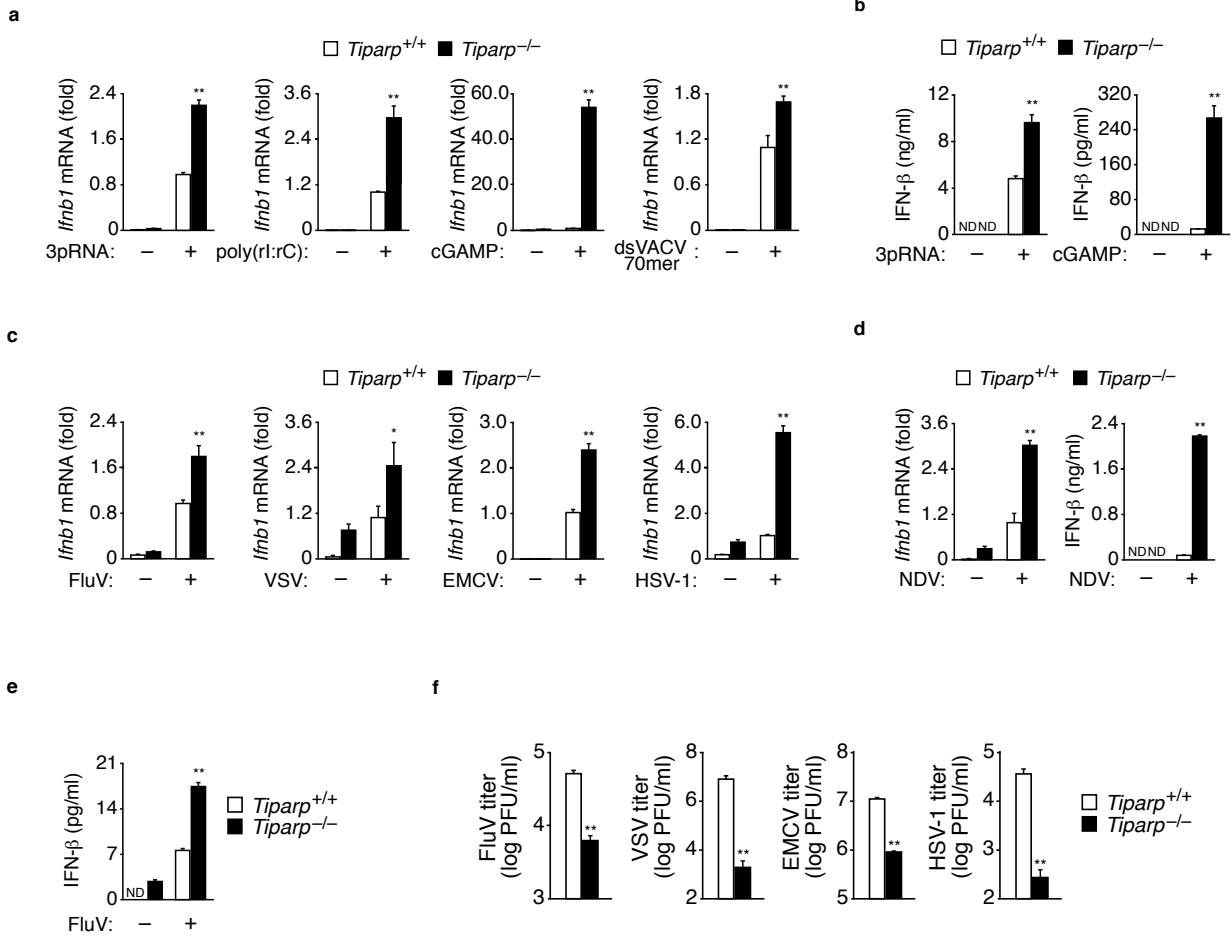

c

d

Figure 3 Yamada *et al.*
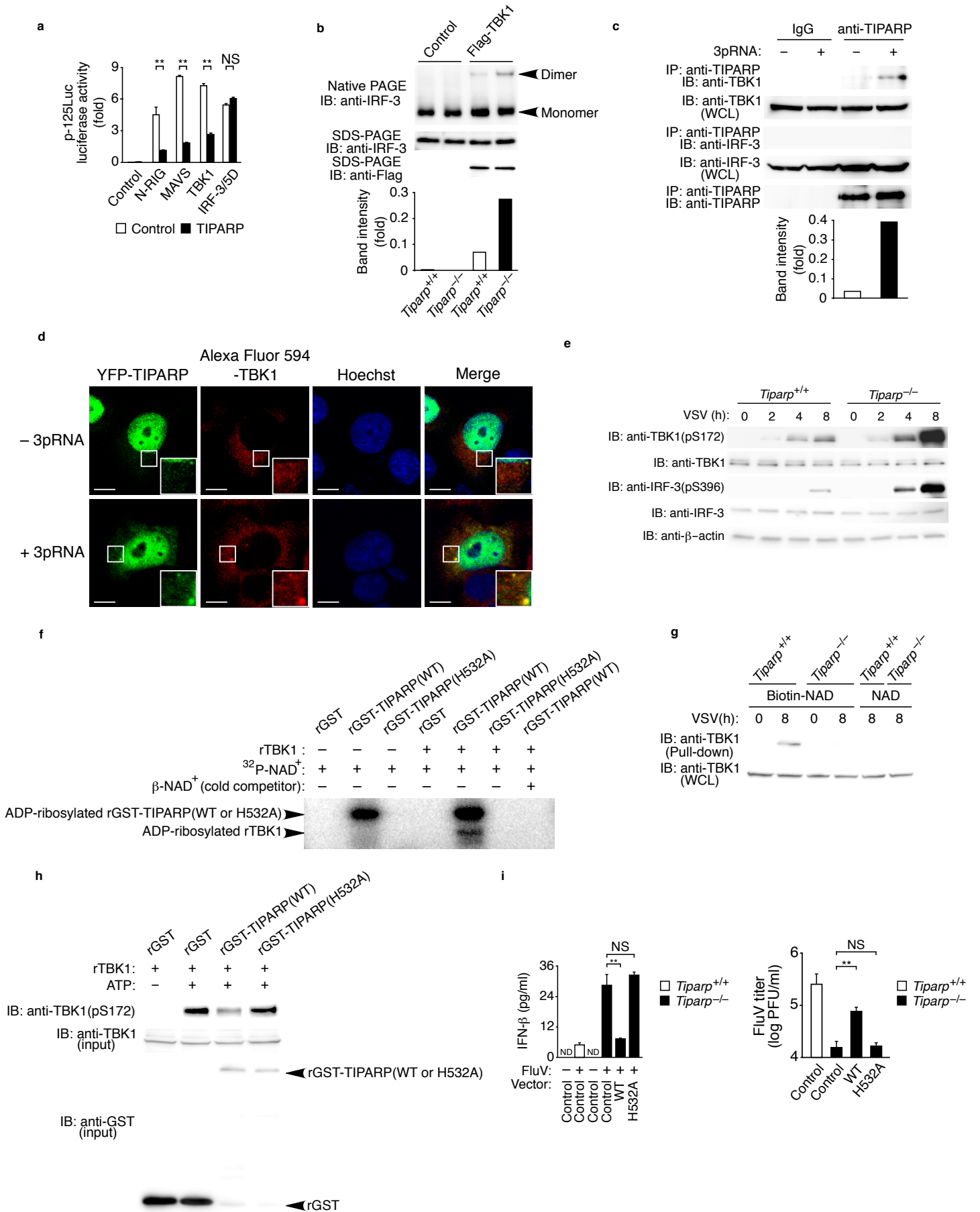
Figure 4 Yamada *et al*.

Figure 5 Yamada *et al*.

Figure 6 Yamada *et al*.